



Combining nanobody generation platform, 3D-printed microfluidic chip, and smartphone detection system for monitoring emerging virus-caused diseases

Yanhong Ji^{a,1}, Fengyun Li^{b,1}, Zhaowei Qu^b, Xiangkun Wang^a, Pengfei Cui^c, Guohua Deng^c, Shaorong Liu², Qiaosheng Pu^{b,*}, Qiyun Zhu^{a,**}, Apeng Chen^{a,d,e,***}

^a State Key Laboratory for Animal Disease Control and Prevention, College of Veterinary Medicine, Lanzhou University, Lanzhou Veterinary Research Institute, Chinese Academy of Agricultural Sciences, Lanzhou, 730000, China

^b State Key Laboratory of Applied Organic Chemistry, Key Laboratory of Nonferrous Metals Chemistry and Resources Utilization of Gansu Province, College of Chemistry and Chemical Engineering, Lanzhou University, Lanzhou, Gansu, 730000, China

^c State Key Laboratory for Animal Disease Control and Prevention, Harbin Veterinary Research Institute, Chinese Academy of Agricultural Sciences, Harbin, 150069, China

^d Department of Respiratory, Children's Hospital of Nanjing Medical University, Nanjing, 210026, China

^e Nanjing Key Laboratory of Pediatrics, Children's Hospital of Nanjing Medical University, Nanjing, 210008, China

ARTICLE INFO

Keywords:

Nanobodies
3D-printed microfluidic chip
H7N9 Detection
Smartphone-Based diagnostics
Point-of-Care Testing (POCT)

ABSTRACT

Rapid in-field detection of emerging viruses is crucial for preventing potential pandemics. This study presents the development of a portable, cost-effective point-of-care testing (POCT) device for detecting emerging pathogens. We took H7N9 avian influenza virus (AIV) as an example, utilizing a combination of novel nanobodies, 3D-printed microfluidic chips, and smartphones to monitor the pathogen. The system employs projection micro-stereolithography (PμSL) 3D printing to fabricate a flower-shaped microfluidic chip, which integrates a micro-pillar array to enhance the surface area for nanobody immobilization. A pair of nanobodies with high specificity and affinity for H7N9 was generated to develop a sensitive colorimetric immunoassay. The assay results can be visually inspected and further quantified using smartphone imaging, eliminating the need for external lighting devices. The device demonstrated a limit of detection (LOD) of 5.9×10^3 EID₅₀/0.1 mL, comparable to traditional ELISA methods, and was validated on real-world samples. The microfluidic chip's reusability was also established, with up to nine reuse cycles without significant loss of sensitivity. The smartphone-integrated POCT device offers the advantages of portability, simplicity, and rapidity, making it a promising tool for in-field H7N9 virus screening, especially in resource-limited settings. This approach exemplifies the potential of integrating advanced nanotechnology with modern manufacturing techniques and ubiquitous devices to enhance diagnostic accessibility and efficiency.

1. Introduction

Viruses are among the most significant pathogens causing global public health threats, with numerous examples of past pandemics, including the H1N1 influenza virus and, most recently, SARS-CoV-2. The

ability of these pathogens to spread rapidly and unpredictably across populations makes them a continual risk to human health. Effective control and prevention of such diseases depend heavily on early and accurate detection of the causative pathogens. However, conventional diagnostic methods, such as virus isolation, enzyme-linked

* Corresponding author.

** Corresponding author.

*** Corresponding author. State Key Laboratory for Animal Disease Control and Prevention, College of Veterinary Medicine, Lanzhou University, Lanzhou Veterinary Research Institute, Chinese Academy of Agricultural Sciences, Lanzhou, 730000, China.

E-mail addresses: puqs@lzu.edu.cn (Q. Pu), zhuqiyun@caas.cn (Q. Zhu), chenapeng@caas.cn (A. Chen).

¹ Authors contribute equally to this work.

² Retired.

immunosorbent assay (ELISA), and reverse transcription polymerase chain reaction (RT-PCR), often require well-equipped laboratories and trained personnel (Okamatsu et al., 2016; Spackman and Killian, 2020) (Leirs et al., 2016; Okamatsu et al., 2016). These limitations make them unsuitable for in-field detection, where a rapid and reliable method is essential to identify potential threats and implement timely interventions (Drain et al., 2014; Schito et al., 2012). To address these challenges, we have developed a versatile point-of-care testing (POCT) platform that integrates a 3D-printed microfluidic chip and a smartphone-based detection system using nanobody-based immunoassays. In this study, we selected the H7N9 avian influenza virus (AIV) as a model pathogen to validate the effectiveness of our method. While H7N9 was chosen as a representative, the system is not limited to this particular virus; it can be easily adapted for detecting other emerging pathogens, making it a promising tool for rapid on-site diagnostics in resource-limited settings.

POCTs have attracted increasing attention because of their in-field usage and timely diagnosis result acquisition (Drain et al., 2014; Schito et al., 2012). Diverse formats of POCTs have been developed to meet different application requirements (Chin et al., 2012), and those based on immunodetection have proven their effectiveness in pathogen detection (Jung et al., 2015). Microfluidics is an ideal technology for POCT because it can miniaturize and integrate an entire process, including sample preparation, separation, reaction, and detection, on a small chip (Gonzalez et al., 2022; Wang et al., 2023). This has many advantages, such as small size, low sample consumption, and fast analysis.

Microfluidics could be further enhanced by applying high-resolution 3D-printing techniques, which greatly simplify the manufacturing process of microfluidic chips (Gonzalez et al., 2022). In those techniques, projection micro-stereolithography (PμSL) is particularly attractive due to its advantage of being suitable for complex and subtle structures (Ge et al., 2020). It has been used to make various structures, such as organs-on-chips (Mi et al., 2018), microneedles (Krieger et al., 2019), flexible electronics (Liu et al., 2021), and bionic functional materials (Kong et al., 2016), which have been used for biomedical sensing (Ali et al., 2022) and POCT (Chan et al., 2017; Yang et al., 2022).

We initially screened to acquire a pair of nanobodies (Nbs) with high affinity and specificity for the H7N9 avian influenza virus to validate our platform. Nbs are derived from the unique single-domain antibodies found in camelids and offer several advantages over traditional antibodies, making them highly suitable for diagnostic applications (Muyldermans, 2021). Their small size (~15 kDa), high stability, and ease of production enable efficient binding to diverse antigens, even in complex environments. Additionally, nanobodies can be easily modified and conjugated with various labels or surfaces, essential for integration into microfluidic systems. Due to these properties, nanobodies have gained increasing attention in diagnostic applications. Their small size allows for efficient diffusion in microfluidic systems, making them ideal candidates for integration into lab-on-a-chip devices.

In this work, we used PμSL 3D printing to construct a flower-shaped microfluidic chip. It was coupled with an easy-to-get imaging element based on two smartphones. The proposed microfluidic device established a cost-effective detection method for pathogens. AIV subtype H7N9, currently circulating in the poultry industry and a public health threat that can directly transmit from birds to humans (Shi et al., 2017), was used as an example to verify the establishment of the microfluidic device. A pair of Nbs F4 and H10, which can recognize different epitopes of H7N9, were generated by our nanobody screening platform in this study and used for immunoassay. A micropillar array (3 × 6) was printed within each microchannel of the microfluidic chip by the PμSL approach to increase the surface area and enhance Nb capturing. We also developed a simple microfluidic chip regeneration procedure to let it be reused at least nine more times. The sensitivity and specificity of the proposed device have been investigated, and a limit of detection (LOD) 5.9×10^3 EID₅₀/0.1 mL was obtained. We further used the microfluidic

device to test the clinical samples, and the results showed it was comparable with the ELISA method. Together, we developed a simple and in-pocket size microfluidic device, which could combine our nanobody-generation platform and potentially be applied for POCT to monitor emerging pathogens.

2. Materials and methods

2.1. Reagents, chemicals, and equipment

2.1.1. Materials of H7N9 and related others

One component 3, 3', 5, 5'-tetramethylbenzidine (TMB) kit and bovine serum albumin (BSA) were from Bioss Biotechnology, China. Ultra-pure water (18.2 MΩ cm, Millipore) was used in the assay. Two three-dimensional (3D) printers were used in the work. The one used for PμSL printing microfluidic chips was microArch®S230, BFM Precision Tech., Chongqing, China; the one used for printing chip bases and boxes for light shading was Whale3 Super, Nova 3D Tech., Shenzhen, China.

2.2. Design and fabrication of 3D-printed microfluidic devices

The 3D structure of the microfluidic chip was designed in Solidworks (Dassault Systèmes, France), and the software exported an '.STL' file. The file was then opened in Voxeldance Additive (version 3.1.6.8, Shanghai, China) and generated its sliced files (the parameters for slicing were as follows: layer thickness 20 μm, pixel 25000 × 25000); the sliced files were then loaded into the microArch®S230 (BMF Precision Tech Inc.) to print the microfluidic chip. The theoretical resolution reported by the manufacturer of this printer is 2 μm. The printer used a 405 nm laser beam to solidify the yellow clear photoreactive resin (HTL Resin, Yellow-5) layer-by-layer to form the complete 3D pattern.

The 3D structure of the chip base, which was utilized to support and protect the microfluidic chip, was designed by Solidworks. The generated '.STL' file was sliced by Novamaker (Shenzhen, China) with the parameters as the layer thickness of 50 μm and the exposure time of 2.0 s; then it was printed by Whale3 Super (Shenzhen Nova Intelligent Technology Co., Ltd, China). The printer used the Chip-On-Board (COB) LED as a light source to solidify the clear and washable photoreactive resin.

The fabrication of the box for light shading when imaging using smartphones was the same as that of the chip base, except that it used grey high-resolution resin. The microfluidic chip was sonicated sequentially in absolute ethanol and ultra-pure water, and the base was sonicated in ultra-pure water. Then, the two parts were air-dried at room temperature and assembled by placing the microfluidic chip in the base.

2.3. Nanobody generation

The generation of nanobodies (Nbs) was conducted following the methods described previously (Shen et al., 2021). Briefly, a healthy alpaca was selected for immunization, with a pre-immunization blood sample collected to separate serum, serving as the negative control. To initiate the immunization protocol, 500 μg of purified H7N9 subtype avian influenza virus HA1 protein was emulsified with an equal volume of Freund's adjuvant. Complete Freund's adjuvant was used for the primary immunization, and subsequent boosts were performed biweekly using incomplete Freund's adjuvant. A total of 5–6 immunizations were administered via multiple subcutaneous injections in the neck area.

Seven days after the final immunization, a blood sample was collected, and an indirect ELISA assay was conducted to assess the antibody titer against the HA1 protein. In this assay, 100 ng of purified HA1 protein was coated per well as the antigen. When the titer of anti-HA1 antibodies reached at least 1:64,000, the phage display nanobody library was constructed.

2.4. Immunofluorescence (IF) and immunoblotting (IB)

Immunofluorescence and immunoblotting assay were performed as described previously (Chen et al., 2021). For the IF assay, human U2OS cells were seeded on coverslips and then infected with AIVs or NDV. The cells were fixed with 4 % paraformaldehyde for 10 min, then permeabilized with 0.3 % Triton X-100 in PBST and blocked with 5 % BSA in PBST for 30 min. The cells were incubated with Nb F4 or H10, followed by incubating with secondary antibodies and counterstaining with DAPI. A confocal microscope (Leica, TCS SP8) was used to detect fluorescence.

For the IB assay, human A549 cells were transfected with an expression vector containing an HA1 construct or infected with AIVs. The cells were lysed on ice in RIPA buffer (Invitrogen) for 30 min. The lysates were separated using 12 % SDS-PAGE gels and transferred to PVDF membranes. The membranes were incubated with HA1 or NP Nbs and subsequently with secondary antibodies. The immunoreactive bands were detected with an ECL system (ThermoFisher).

2.5. Surface plasmon resonance (SPR) assay

The affinities of Nbs to HA1 or AIVs were measured using Biocore 8 K equipment (Cytiva). An Nb recognizing a different epitope of HA1 protein was immobilized onto the CM5 sensor surface by following the standard amine-coupling process based on the manufacturer's protocol. PBST buffer was used as the running buffer. After capturing the HA1 protein or H7N9 viruses, the analytes (Nb F4 or H10) were measured using a two-fold serial dilution. The injection was performed with a flow rate of 20 mL/min, followed by 180 s dissociation time. The data were collected and fitted to a 1:1 binding kinetics model to calculate the equilibrium dissociation constant (K_D) using Biacore Software (Cytiva).

2.6. Characterization of the microfluidic chip

The microstructures of the microfluidic chip were characterized by the laser spectroscopic confocal microscope (KC-X1000, KathMatic). To observe the microstructures inside the chip, the microfluidic chip was partly printed from the bottom layer up to the micropillars with 100 μ m height, so the microstructures initially inside the chip were exposed outside. They were imaged by the laser spectroscopic confocal microscope. The partly printed chip was also used to characterize the micro-morphology of the microfluidic chip by field emission scanning electron microscopy (SEM, S-4800, Hitachi, Japan).

2.7. Immunoassay on the microfluidic chip

The capture Nb F4 was physically absorbed on the inner surface of the microchannels. 20 μ L of Nbs (diluted in carbonate buffer, pH 9.6) was pipetted into each inlet and incubated at 4 °C for overnight. The chip was placed in a covered Petri dish with a wet sponge to prevent excessive solution evaporation. Before use, the solution was blown out by a rubber pipette bulb through the central inlet. 200 μ L of BSA (5 % in PBST solution) was injected into the central inlet; the solution was left at room temperature for 5 min. Then, 20 μ L of the mixture of H7N9 viruses and horseradish peroxidase (HRP) labeled recognized Nb H10 was added and incubated at 37 °C. Subsequently, 200 μ L of PBST was injected into the central inlet, incubated at room temperature for 1 min, and then blown out. This step was repeated five times. Finally, 20 μ L of TMB solution was added and incubated at 37 °C for 10 min. The microchip was placed on the bright screen of one smartphone (Huawei Nova) and imaged by another (Honor Magic5 Pro). The images were processed by the RGB grab program (Li et al., 2022).

After each test, the microfluidic chip was sonicated in a saturated laundry detergent solution (about 160 g in 1 L ultra-pure water) for 20 min, followed by washing in ultra-pure water. It was then sonicated again in absolute ethanol for 5 min and air dried at room temperature.

2.8. Washing evaluation of microfluidic chip

The surface micromorphologies of the microfluidic chips after coating with a nanobody, blocking with BSA, incubating with H7N9/HRP-Nb, and final washing with the laundry detergent solution were characterized by an atomic force microscope (AFM, Bruker Dimension Icon, Bruker, America). To mimic the surfaces of the microchannel and be easily observed by the equipment, four 3D-printed wafers (printer BFM microArch®S230, diameter: 1 cm, thickness: 1 mm) were used.

All the wafers were immersed in CB buffer and washed with ultra-pure water. One wafer was stored for characterization; the other three were coated by captured Nb at 4 °C overnight, followed by rinsing with ultra-pure water; then, one wafer was stored for characterization; the other two were incubated with the mixture of H7N9 and HRP-recognized Nb at 37 °C for 2 h, followed by washing with ultra-pure water; subsequently, one wafer was stored for characterization, and the last one was then washed with the steps as mentioned in **Immunoassay on microfluidic chip**. All four wafers were characterized by the AFM using the ScanAsyst model.

2.9. Limit of detection (LOD), sensitivity, and dynamic range

LOD was calculated in this manuscript according to the most accepted and used formula: $S_{LOD} = S_{blank} + 3 \times SD_{bl}$, Where S_{LOD} is the minimum distinguishable signal, S_{blank} is the mean blank signal, and SD_{bl} is the standard deviation of the blank. Then, LOD was calculated from the calibration equation according to the curve plotted by the signal versus the concentration of H7N9 in log10 form of EID_{50} . Sensitivity was calculated with the following equation: $S = mc + S_{bl}$, where S is the measured signal, c is the concentration of the analyte, S_{bl} is the instrumental signal for a blank, and m is the slope of the straight line. Dynamic range was determined by LOD and the concentration at which the calibration curve departs from linearity (limit of linearity, LOL).

2.10. Specificity evaluation assay

Five types of viruses, including AIV subtypes H3N2, H5N6, H6N6, and H9N2, and a common poultry virus—a new cattle virus (NDV)—were twofold diluted in PBST from the original stock, and the final concentrations were approximately 5×10^7 $EID_{50}/0.1$ mL. All viruses were analyzed as the H7N9 mentioned above (see details in **Immunoassay on microfluidic chip**). For comparison, H7N9 was used at 5.0×10^5 $EID_{50}/0.1$ mL. The selectivity was further calculated from the equation as follows: $S = m_A c_A + m_B c_B + m_C c_C + \dots + S_{bl}$, where A is the analyte H7N9, B, C, and ... are potential interfering species (i.e., H3N2, H5N6, H9N2, and NDV). We took all references to the same concentration and assumed they have a similar m to calculate the selectivity coefficient, $k_{B,A} = m_B/m_A$.

2.11. Real-world sample test

Chickens were infected with H7N9, and the organs were collected for detection. The chickens without infection were the control group. For the mixed samples, the organs from the same chicken were collected and mixed; a mixed sample included the liver, lungs, kidney, spleen, pancreas, trachea, and pancreas from the same animal. For separate detection, another batch of chickens is infected or without infection. The organs were separately collected and tested. The detection procedures were similar to the **Immunoassay on the microfluidic chip** mentioned above, except the samples were separately added from the HRP-nanobody; that is, the samples were added to the chip first and incubated for 1 h at 37 °C, and then the HRP-nanobody solution was added for incubating another 1 h. The real-world samples were used directly after preparation to mimic the manipulation in practice.

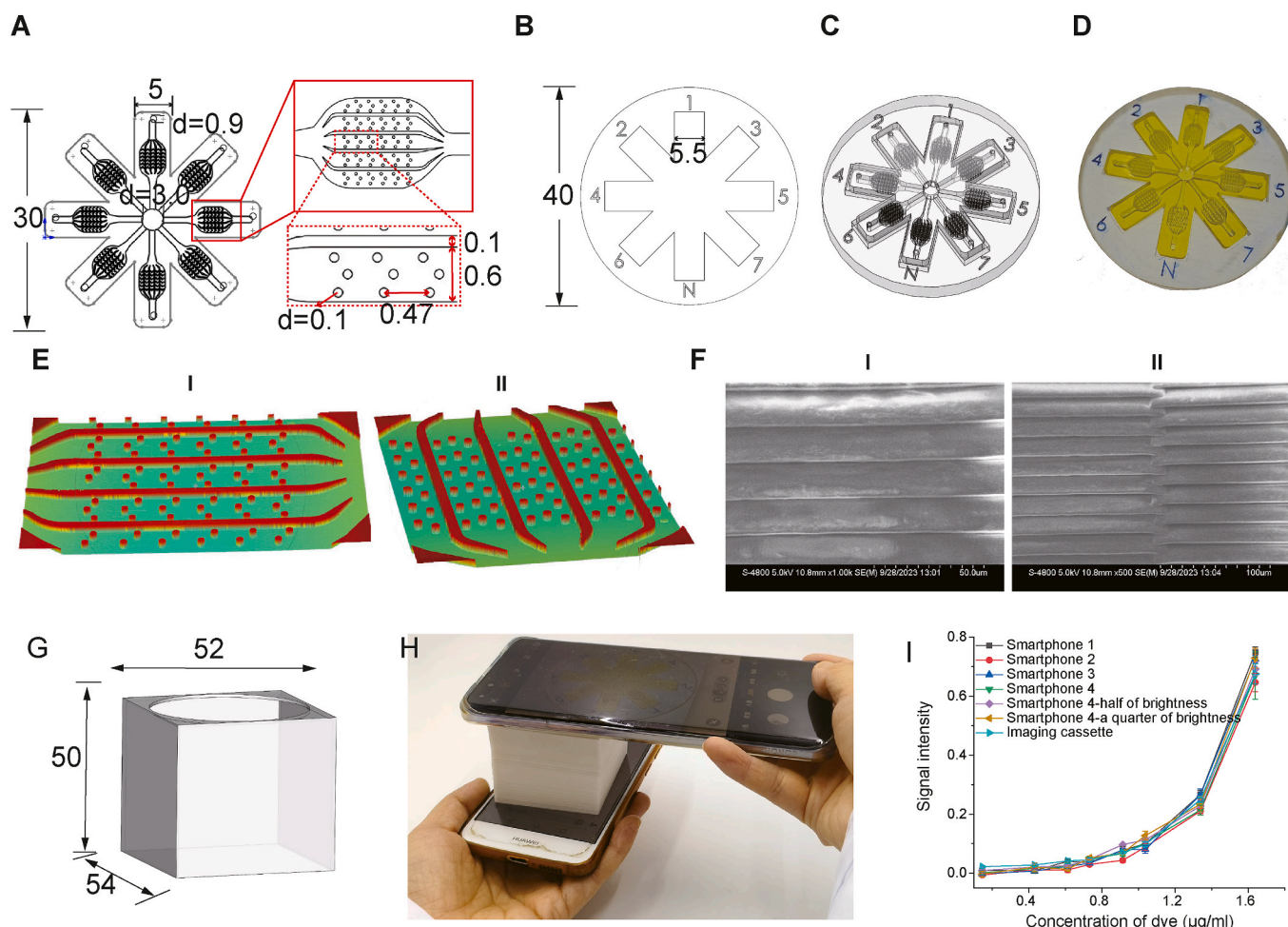


Fig. 1. Design and principle of the microfluidic device. (A) Scheme of the core microfluidic chip, the top right and bottom right sections were enlarged schemes of a set of microchannels and a single microchannel. (B) Scheme of the microchip base. (C) Scheme of the integrated microfluidic chip with the core and the base. (D) The photo of an actual microchip. (E) The inner images (I and II) of a set of microchannels from a laser spectroscopic confocal microscope. (F) The SEM characterization of the inner wall surfaces of the microchannel (I for microchannel and II for micro-circular pillar). (G) Schematic illustration of the 3D printed box. (H) Image of using two smartphones. (I) Evaluation of different brand smartphones and screen brightness on the imaging results. Error bars represent standard deviations ($n = 5$). The units of the numbers are mm.

2.12. Establishment of the homemade ELISA

50 μ L of capture Nb F4 diluted in carbonate buffer (pH 9.6) with the concentration 0.4 μ g/mL was added into a 96-well microtiter plate (Corning) and incubated at 4 $^{\circ}$ C overnight. The solution was discarded, and the plate was washed twice with 300 μ L of PBST (0.1 % tween-20). 300 μ L of BSA (5 % in PBST, v/v) was added into each well of the plate for blocking at 37 $^{\circ}$ C for 2 h. After washing twice with PBST, 50 μ L of H7N9 virus was added into each well at 37 $^{\circ}$ C for 1 h. After washing three times with PBST, 50 μ L of HRP-Nb H10 (1.1 μ g/mL) were added to the wells and incubated at 37 $^{\circ}$ C for 1 h. Then, washed five times with PBST, 50 μ L of TMB substrates were added and incubated at 37 $^{\circ}$ C for 10 min. The signals were recorded by a microplate reader (Tecan, Switzerland).

3. Results and discussion

3.1. Design and construction of microfluidic device

To make the manipulation convenient for pathogen detection, the microfluidic chip was designed as a flower shape, as shown in Fig. 1A, with a size of 30 mm \times 30 mm \times 2.4 mm (length \times width \times height). It has eight symmetrically distributed petals with a width of 5.0 mm each.

The petal is composed of five microchannels where the immunoassay was performed. The microchannel has a dimension of 3.2 mm \times 0.8 mm \times 1.6 mm, and the microchannels are separated with a partition thickness of 0.12 mm. In each microchannel, micro-circular pillars (3 \times 6, diameter 0.1 mm and height 1.6 mm) were designed to increase the surface-to-volume ratio. In the center of the microchip, a hole with a diameter of 3.0 mm was designed for the injection of wash solution. At the ends of each petal, sampling holes with a diameter of 0.9 mm were designed for adding samples and reagents.

Additionally, a round base with a diameter of 40 mm and a height of 4.0 mm was designed (Fig. 1B). It has the same contour as the flower-shaped microfluidic chip. The function of the base is to serve as a reservoir (with a depth of 2.0 mm) of the microfluidic chip, as shown in Fig. 1C. The reservoir can prevent scratches of the chip during manipulation and also conveniently label petals of the microfluidic chip as from 1 to 7, or N (Fig. 1C). Note that the width of each petal of the reservoir is 5.5 mm, which is slightly wider than the petal of chip, to make they can fit rightly and tightly. The constructed microfluidic chip setting in the reservoir is shown in Fig. 1D.

To observe whether the 3D printer correctly constructed the microfluidic chip, we utilized a laser spectroscopic confocal microscope to characterize the inner wall of the microchannels. As shown in Fig. 1E, the microstructures, including micropillars, partitions, and

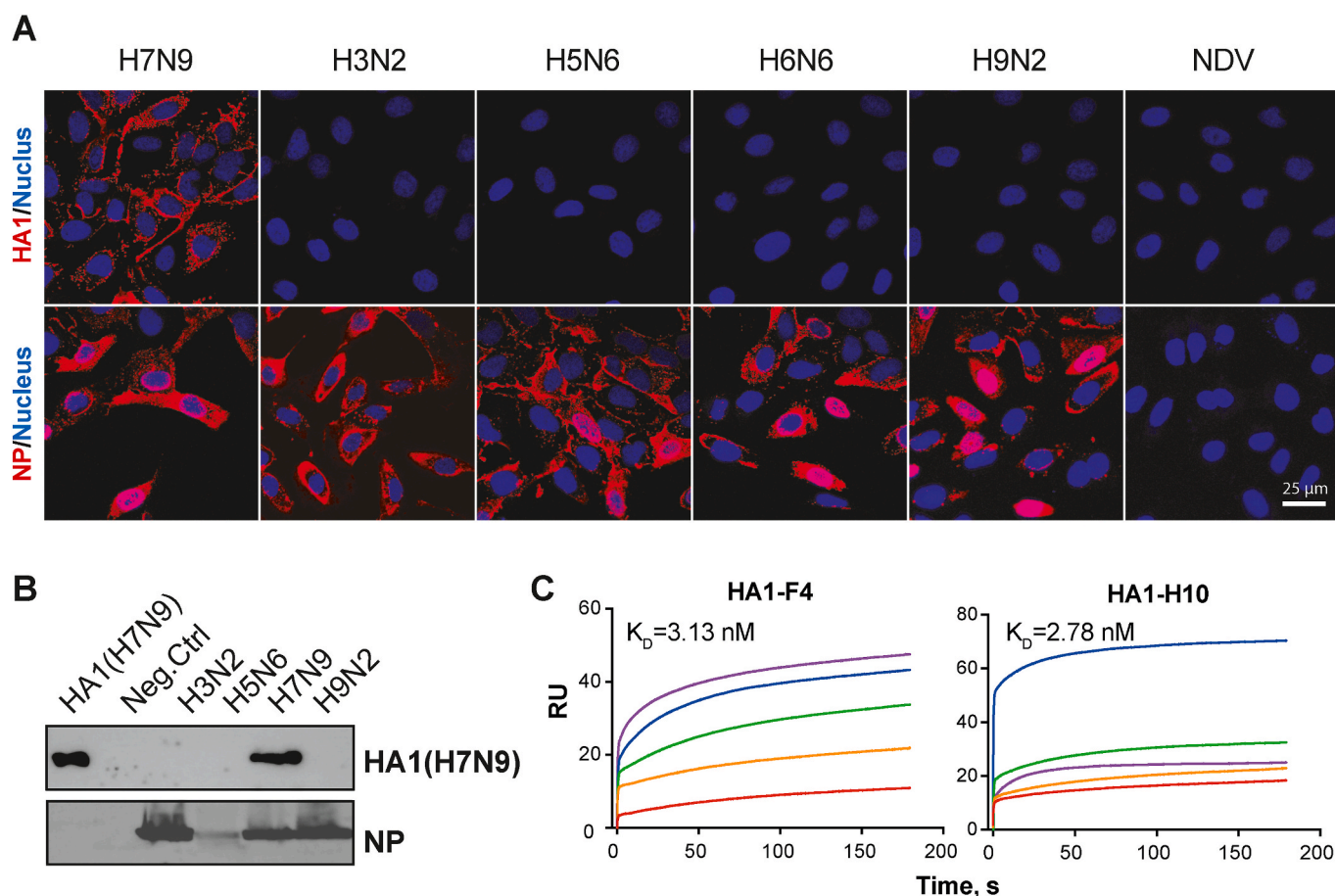


Fig. 2. The specificity and affinity of the Nbs. (A) U2OS cells were infected with different IAV subtypes or NDVs; the infected cells were detected by H7N9 HA1-specific Nb F4 or a broadly IAV NP recognized Nb 204. (B) A549 cells were transfected with a H7N9 HA1-expressing plasmid or infected with different IAV subtype viruses; the cells were detected by Western blot with H7N9 HA1-specific Nb F4 or a broadly IAV NP recognized Nb 204. (C) The affinity of Nbs F4 and H10 to H7N9 HA1 was acquired with SPR. The coating concentrations for F4 are 5.93, 11.87, 23.75, 47.50, 95.00, and 190.00 nM, while for H10 are 13.43, 26.88, 53.75, 112.50, and 215.00 nM, followed by 180s dissociation time.

microchannels, were printed entirely—they had clear boundaries, and the micropillars were distributed uniformly, suggesting that a satisfied microfluidic chip could be well produced by high-resolution PμSL 3D printing. We further characterized the microstructure surface of the microchannel with SEM. As shown in Fig. 1F, a clear and uniform-layered structure was demonstrated, which is consistent with microstructures by other 3D printings (Mostafa et al., 2020; Subirada et al., 2022). The roughness of the sidewall, derived from the layered structure, would provide a sufficient surface to increase the capacity of absorbing antibodies on the wall, which is critical to enhancing the sensitivity of the immunoassay.

To collect immunoassay results timely at the point of care, we designed a convenient system composed of a light-shield box (Fig. 1G) and two smartphones (Fig. 1H). The light-shield box was made by a 3D printer (Nova Whale 3 Super). It has a dimension of 54 mm × 54 mm × 50 mm (length × width × height) and a round hole with a diameter of 52 mm. The bottom smartphone, as shown in Fig. 1H, served as an ambient light source, and the top smartphone could capture the images of a microfluidic chip setting in the box with its camera. Four smartphone brands were tested to investigate whether different smartphones could produce varied light brightness from their screen (Fig. 1I). The LED-based imaging reader constructed in our previous work (Li et al., 2022) was used as a control. As a result, all the smartphone screens displayed similar performance under the highest brightness. When the brightness is decreased to half or a quarter, the performance can still satisfy the requirement, suggesting that the brightness and resolution of

smartphone screens have little influence on the results. Its good performance is because the RGB grab program we used has a flexible tolerance range to light brightness, after the exported signals from the RGB grab program have been subtracted backgrounds (Li et al., 2022). The detection instrument can be simply substituted with two smartphones in the system.

3.2. Characterization of nanobodies

To generate suitable nanobodies that can be used for immunoassay, we immunized AIV H7N9 HA1 protein as an antigen to an alpaca. We followed the steps described previously (Shen et al., 2021) to screen and produce H7N9-specific Nbs (see details in the Materials and methods). We acquired two Nbs, F4 and H10, with good specificity and high affinity to H7N9 subtype viruses. As shown in Fig. 2A and B, and Fig. S1A, the two Nbs specifically recognized the AIV H7N9 subtype rather than other common subtypes, including H3N2, H5N6, H6N6, and H9N2, suggesting they were suitable for developing immunoassays. We further measured the affinity of the two Nb to H7N9 HA1 protein by SPR (Fig. 2C). The results showed that Nb F4 has a K_D of 3.13 nM and Nb H10 a K_D of 2.78 nM to HA1, respectively. Since HA1 protein is the hemagglutinin of AIV, which is part of the virus particles, we additionally tested whether the Nbs, F4 and H10, have a similar affinity to the whole virus particle. The SPR results showed the two Nbs have a closed affinity to the virus particles (Fig. S1B). Together, the generated two Nbs have high specificity and affinity for immunoassays.

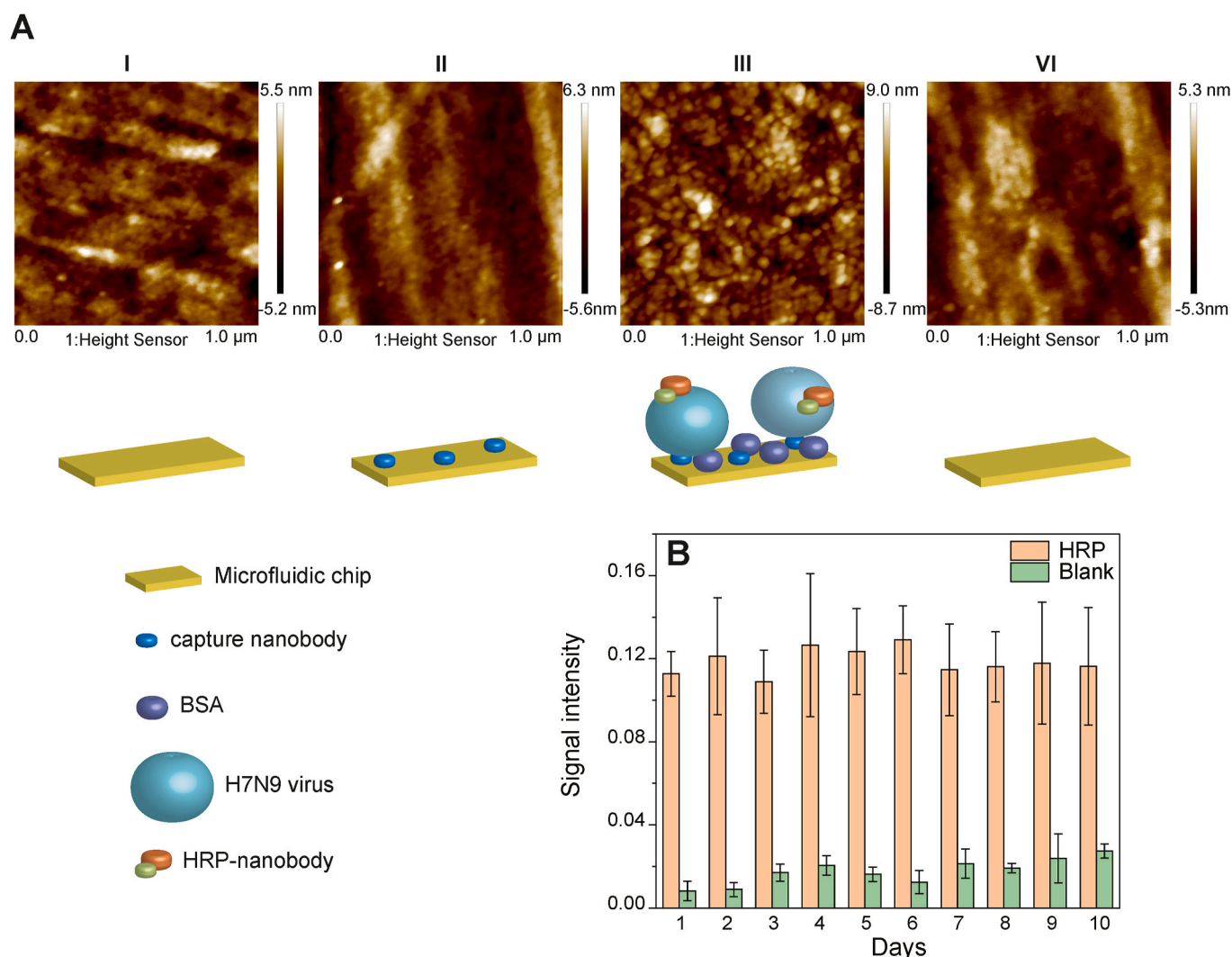


Fig. 3. (A) Characterization of the surface morphology of microchips under four stages by AFM. (B) HRP is used as a model for evaluating wash treatment cycles on the re-use of microchips. Error bars represent standard deviations ($n = 5$).

3.3. Regeneration of the microfluidic chip

To reduce the cost and shorten experimental cycles in practice, we explored the regeneration of microchips. Commercial laundry detergent has been widely used to remove diverse organic and inorganic contaminations, it was also used to eliminate the substances like proteins bounded on the PμSL 3D-printed microchannel inner-surface after a test and hence the microchip might be reusable. Briefly, microfluidic chip regeneration includes sonication in a laundry detergent solution and, subsequently, absolute ethanol, followed by air drying. To evaluate whether it could remove substances bounded on the microchannels derived from photo-curing of acrylate resin by PμSL 3D-printer, the surface morphology of the microfluidic chip was further characterized by AFM. As shown in Fig. 3A, the surface of the microchip immersed in CB buffer was relatively smooth (stage I); the surface coated with captured nanobody displayed similar morphology (stage II), which was probably due to the small molecule weight of Nbs; after BSA blocking and incubation with the mixture of H7N9 and HRP-nanobody, there were a large number of regular spherical particles on the surface (stage III); finally, the surface (stage IV) showed the similar morphology as stage I and II after washing, suggesting the microfluidic chip was well regenerated.

Next, to further confirm the reusability after regeneration treatment, we used HRP-labeled Nbs to evaluate the coating efficiency of the

regenerated microfluidic chip by assessing the blue color produced by HRP. As shown in Fig. 3B, the colorimetric signal values were consistent between the newly printed microfluidic chip (cycle 1) and the other nine re-used microfluidic chips (cycle 2–10), indicating that the microchip has recovered its ability to absorb HRP-labeled Nbs after the regeneration procedures. One should note that the background signal slightly increased gradually with the re-used cycles, although there was no significant statistical difference. We suggest that one regenerate the microfluidic chips no more than nine times.

3.4. H7N9 subtype AIVs immunoassay

To evaluate its practical applications in monitoring emerging viruses, we used the microfluidic device to detect H7N9 subtype AIVs as a representative, which have been circulating in the poultry industry. The portable microfluidic device was integrated with a 3D-printed microfluidic chip and smartphones. Before the test, we investigated the two most essential immunoassay conditions: immuno-reaction time and amounts of nanobodies (Fig. S2). The incubation time of the mixture of H7N9 viruses and HRP-labeled Nb H10 and pre-coated capture Nb F4 was evaluated. The data showed that 1.5 h would be the optimized incubation time, which produced the maximum and stable signals (Fig. S2A). We further investigated the effects of Nb concentrations on signals (Fig. S2B and C). For capture Nb F4, the concentrations from 0.4

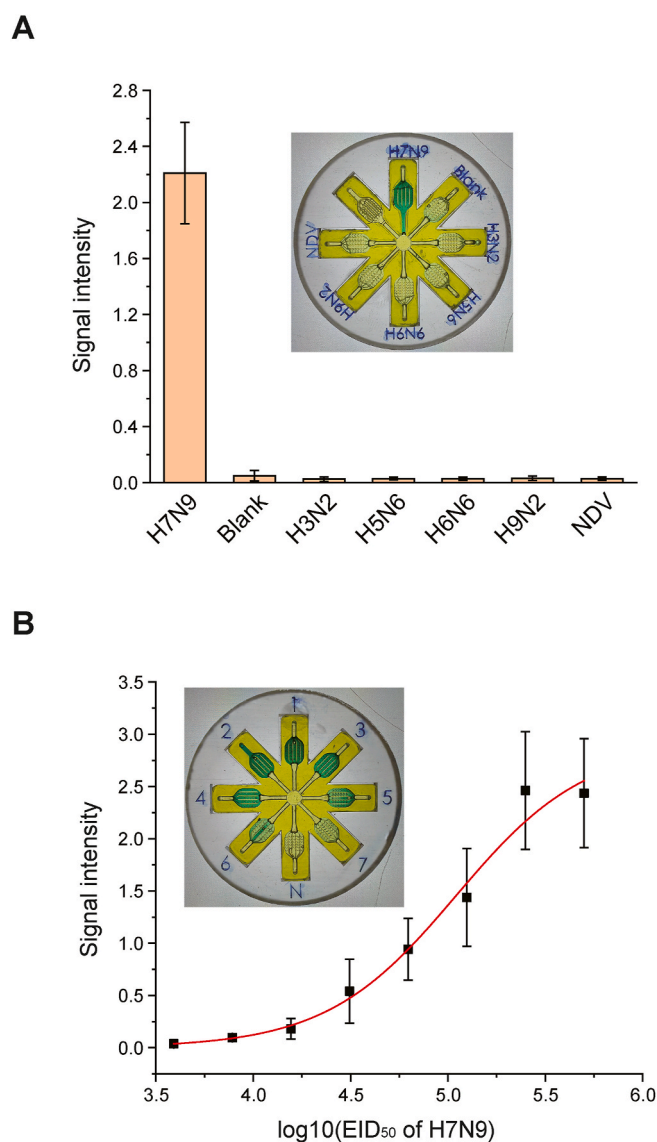


Fig. 4. (A) Evaluation of the specificity of the microfluidic device and the inset was a typical image of the microchip. (B) Detection of the H7N9 virus using the microfluidic device, and the inset was a typical image of the microchip. Error bars represented standard deviations ($n = 5$).

to 10 $\mu\text{g/mL}$ did not influence positive signals and background (i.e., S/N), suggesting that the 0.4 $\mu\text{g/mL}$ of Nbs is sufficient to catch H7N9 viruses. We used 0.4 $\mu\text{g/mL}$ of capture Nb F4 in the following experiments to reduce the cost. For detecting Nbs (i.e., HPR-labeled Nb H10), data showed the concentration of 1.1 $\mu\text{g/mL}$ had the best signals and ignored background; hence, we used this concentration in the following experiments.

3.5. The selectivity and sensitivity

To test the selectivity of the developed microfluidic device, we investigated the specificity of the detection of AIV subtype H7N9 from other AIV subtypes, including H3N2, H5N6, H6N6 and H9N2 (Fig. 4A). We also included new cattle virus (NDV), which is also common in the poultry industry. The results showed that only H7N9 had a strong signal, while the others had low signals, the same as the blank. Theoretically, one can easily switch to detect pathogens as long as the specific Nbs developed with the described Nb-producing platform.

Next, we analyzed the performance range of the microfluidic device

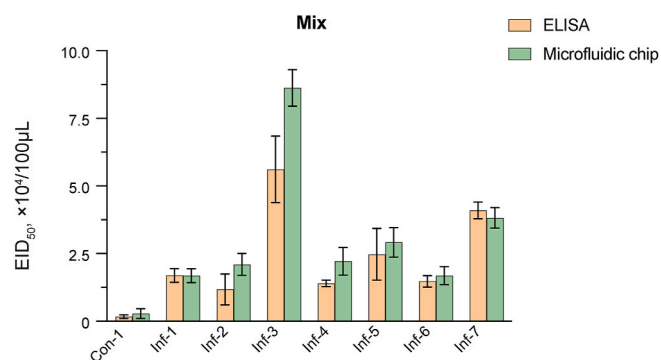


Fig. 5. Comparison of ELISA and microfluidic device detection on chicken mix viscera samples. Error bars represented standard deviations ($n = 3$ for ELISA and $n = 5$ for microfluidic device).

for detecting H7N9 subtype viruses. The signals from a series of concentrations of the H7N9 were examined. As illustrated in Fig. 4B, the blue color derived from HRP catalyzation gradually deepened as the concentration of H7N9 on the chip increased (see the inset of the microfluidic chip of Fig. 4B). The signals were captured as a photo by the smartphone and further processed by the RGB grab program (Li et al., 2022). The signals were plotted against the H7N9 concentration in log₁₀ format; a good sigmoidal relationship was obtained in the range of $0.5.0 \times 10^5$ EID₅₀/0.1 mL with a correlation coefficient of $R^2 = 0.9910$ (Fig. 4B). As a result, the estimated limit of detection (LOD) of the microfluidic device for H7N9 was 5.9×10^3 EID₅₀/0.1 mL according to the average blank signal plus three times of its standard deviation (Belter et al., 2014) from the experimental results.

The detection sensitivity for the H7N9 was also evaluated by the ELISA using the same pair of nanobodies. The ELISA also produced a good sigmoidal relationship in the same concentration range as above ($R^2 = 0.9974$, Fig. S3), and a calculated LOD 4.2×10^3 EID₅₀/0.1 mL according to the three times of signal-to-noise ratio. The results from the microfluidic system were comparable with the ELISA method, demonstrating the proposed microfluidic system can detect the H7N9 subtype viruses. The detection results were also in the similar level with those previous reported immunochromatographic strip tests, but predominated in its simple design and portability compared with those diverse techniques which either use sophisticated instrumentation or special designs with materials in signal amplification (Table S1). The calibration sensitivity was further determined based on Fig. 4B as 1.19–1.27/ $\log_{10}(\text{EID}_{50})$, and the selectivity for other references (i.e., IAV subtypes and NDV) is approximately -0.12 when those references are at very high concentration, suggesting the Nbs have good selectivity for H7N9. Additionally, the dynamical range was determined to be $5.90 \times 10^3 \sim 5.62 \times 10^5$ EID₅₀, which overlaps with the clinical range of IAVs in the avian industry in practice. Since it is portable and can be carried in a pocket, the microfluidic device could be easily used at the point of care.

3.6. Application of the microfluidic device

To demonstrate the utility of the developed microfluidic device for real-world samples, we used it to detect H7N9 subtype virus-infected vs. non-infected poultry. As shown in Fig. 5, the organs of the infected chicken were mixed, and then the EID₅₀ of the viruses was measured by a microfluidic device. The samples were also tested by using the ELISA assay. Six of the seven infected samples showed similar detection results, and one sample (Inf-3) showed higher signals detected by the microfluidic device than by the ELISA assay. The data suggest that detection by the microfluidic device is comparable to the ELISA method in practice.

Since AIVs infect chicken organs with different efficiency, we further measured the virus titers in organs separately, including the liver, lung,

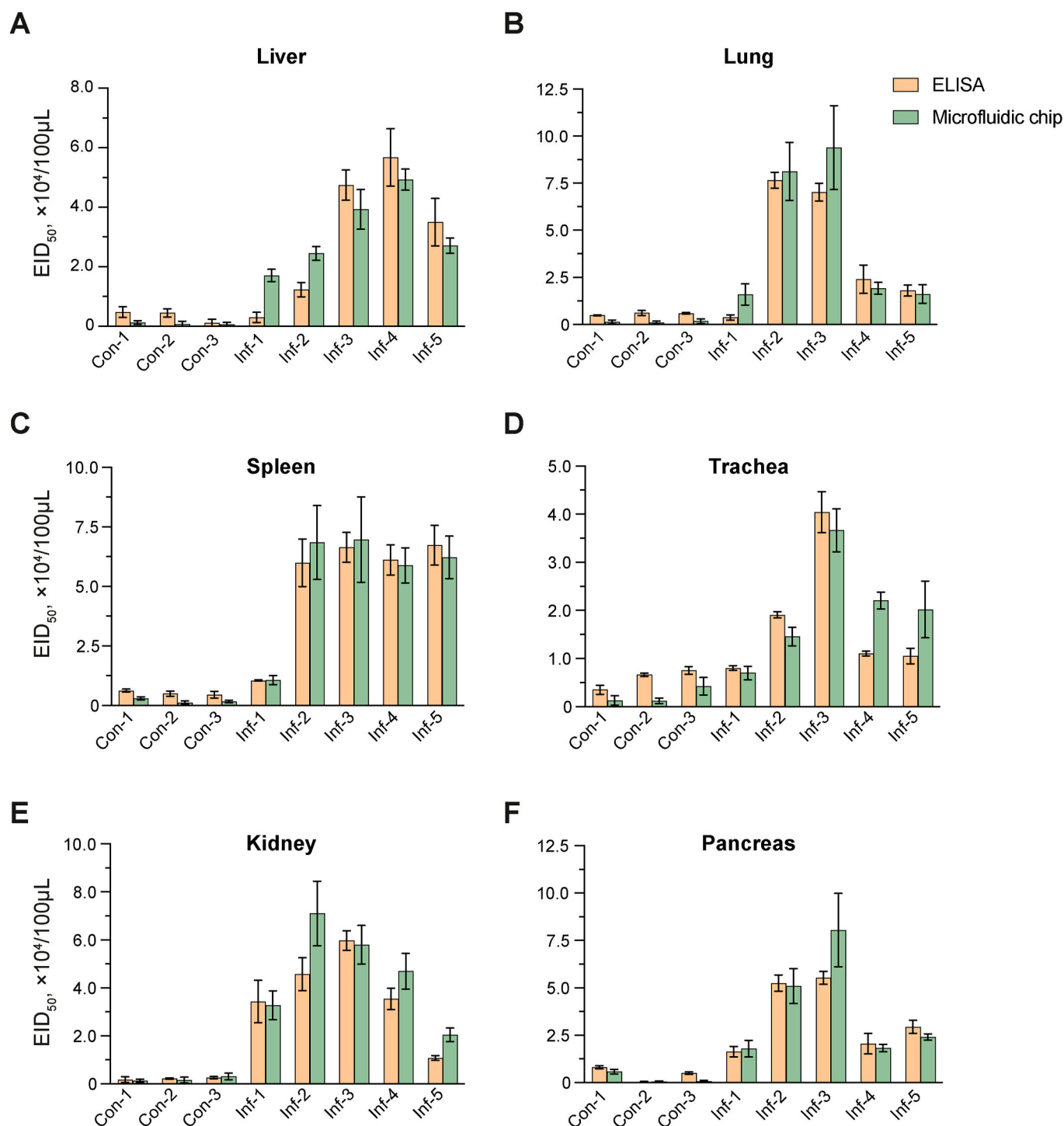


Fig. 6. Comparison of ELISA and microfluidic device detection on chicken samples from liver (A), lung (B), spleen (C), trachea (D), kidney (E), and pancreas (F). Error bars represented standard deviations ($n = 3$ for ELISA and $n = 5$ for microfluidic device).

spleen, trachea, kidney, and pancreas (Fig. 6). The microfluidic device was used to test another batch of five chickens infected with H7N9 vs. three without infection, and the ELISA assay was used for comparison. The results showed the measurement by the microfluidic device is comparable with the ELISA assay; occasionally, our microfluidic device got even a little higher signal than those by the ELISA assay, suggesting that the microfluidic device has potential application in clinical diagnosis.

Finally, it is necessary to emphasize that the major purpose of detecting H7N9 from practical samples is to verify the Nb-producing

platform and prototype of the developed microfluidic device can be integrated seamlessly for real-world applications. When an unknown or new pathogen emerges and becomes a pandemic, one should be able to screen and generate specific Nbs and use them in the microfluidic device to develop a detection method for the pathogen.

4. Conclusions

We proposed a pocket-size microfluidic device comprising two smartphones and a PμSL 3D-printed microfluidic chip. We screened a

pair of high-specificity and affinity Nbs for H7N9. By integrating them, we established a fast, portable, cost-effective, and simple colorimetric immunodetection method for detecting H7N9 subtype AIVs. However, this selection does not limit the system's applicability, as our method can be adapted for detecting a wide range of viral pathogens by simply replacing the nanobody pair with those targeting other pathogens.

The 3D-printed microfluidic chip had an array of micropillars within each microchannel to provide an increased surface area for absorbing sufficient Nbs, a critical strategy for improving detection sensitivity. In addition, we proved that the smartphone screen provided comparable images with LED screens by subtracting the background, so two smartphones are enough when imaging the colored microfluidic chip without the external construction of a light source. In sum, we demonstrated a POCT-pathogen-monitoring system by integrating the Nb screening/producing platform and the developed microfluidic device. Integrating Nbs in our microfluidic POCT device enables rapid, sensitive, and specific pathogen detection in a portable and user-friendly format, making it highly versatile for potential field applications.

CRedit authorship contribution statement

Yanhong Ji: Writing – review & editing, Writing – original draft, Validation, Resources, Methodology, Investigation, Funding acquisition, Conceptualization. **Fengyun Li:** Writing – review & editing, Writing – original draft, Visualization, Validation, Resources, Methodology, Investigation, Formal analysis, Data curation, Conceptualization. **Zhaowei Qu:** Validation, Investigation. **Xiangkun Wang:** Validation. **Pengfei Cui:** Resources. **Guohua Deng:** Resources. **Shaorong Liu:** Writing – review & editing. **Qiaosheng Pu:** Supervision, Software, Resources, Project administration, Data curation, Conceptualization. **Qiyun Zhu:** Supervision, Resources, Project administration, Funding acquisition. **Apeng Chen:** Writing – review & editing, Writing – original draft, Visualization, Supervision, Methodology, Funding acquisition, Formal analysis, Conceptualization.

Declaration of competing interest

The authors declare that they have no known competing financial interests or personal relationships that could have appeared to influence the work reported in this paper.

Acknowledgments

This work was supported by the Major Science and Technology Project of Gansu Province (23ZDNA007, 22ZD6NA001, and 21ZD3NA001-13), the National Natural Science Foundation of China (32273019, U23A20243, and 32272972), Centrally Guided Local Science and Technology Development Special Fund Project (23ZYQA295), the Key Research and Development Plan of Gansu Province - International Cooperation Field (24YFWA008), the Agricultural Science and Technology Support Project of Gansu Province's Department of Agriculture and Rural Affairs (KJZC-2024-33), and East-West Science and Technology Cooperation Special Project (Jin-Gan and Lu-Gan Cooperation) (24CXNA031). The graphical abstract was created with [BioRender.com](https://www.biorender.com) with modifications.

Appendix A. Supplementary data

Supplementary data to this article can be found online at <https://doi.org/10.1016/j.bios.2025.117972>.

Data availability

Data will be made available on request.

References

- Ali, M.A., Hu, C., Yttri, E.A., Panat, R., 2022. Recent advances in 3D printing of biomedical sensing devices. *Adv. Funct. Mater.* 32, 2107671. <https://doi.org/10.1002/adfm.202107671>.
- Belter, M., Sajnóg, A., Baralkiewicz, D., 2014. Over a century of detection and quantification capabilities in analytical chemistry – historical overview and trends. *Talanta* 129, 606–616. <https://doi.org/10.1016/j.talanta.2014.05.018>.
- Chan, H.N., Tan, M.J.A., Wu, H., 2017. Point-of-care testing: applications of 3D printing. *Lab Chip* 17, 2713–2739. <https://doi.org/10.1039/C7LC00397H>.
- Chen, A., Jiang, Y., Li, Z., Wu, L., Santiago, U., Zou, H., Cai, C., Sharma, V., Guan, Y., McCarl, L.H., Ma, J., Wu, Y.L., Michel, J., Shi, Y., Konnikova, L., Amankulor, N.M., Zinn, P.O., Kohanbash, G., Agnihotri, S., Lu, S., Lu, X., Sun, D., Gittes, G.K., Wang, Q., Xiao, X., Yimlamai, D., Pollack, I.F., Camacho, C.J., Hu, B., 2021. Chitinase-3-like 1 protein complexes modulate macrophage-mediated immune suppression in glioblastoma. *J. Clin. Investig.* 131. <https://doi.org/10.1172/JCI147552>.
- Chin, C.D., Linder, V., Sia, S.K., 2012. Commercialization of microfluidic point-of-care diagnostic devices. *Lab Chip* 12, 2118–2134. <https://doi.org/10.1039/C2LC21204H>.
- Drain, P.K., Hyle, E.P., Noubary, F., Freedberg, K.A., Wilson, D., Bishai, W.R., Rodriguez, W., Bassett, I.V., 2014. Diagnostic point-of-care tests in resource-limited settings. *Lancet Infect. Dis.* 14, 239–249. [https://doi.org/10.1016/S1473-3099\(13\)70250-0](https://doi.org/10.1016/S1473-3099(13)70250-0).
- Ge, Q., Li, Z., Wang, Z., Kowsari, K., Zhang, W., He, X., Zhou, J., Fang, N.X., 2020. Projection micro stereolithography based 3D printing and its applications. *Int. J. Extrem. Manuf.* 2, 022004. <https://doi.org/10.1088/2631-7990/ab8d9a>.
- Gonzalez, G., Roppolo, I., Pirri, C.F., Chiappone, A., 2022. Current and emerging trends in polymeric 3D printed microfluidic devices. *Addit. Manuf.* 55, 102867. <https://doi.org/10.1016/j.addma.2022.102867>.
- Jung, W., Han, J., Choi, J.-W., Ahn, C.H., 2015. Point-of-care testing (POCT) diagnostic systems using microfluidic lab-on-a-chip technologies. *Microelectron. Eng.* 132, 46–57. <https://doi.org/10.1016/j.mee.2014.09.024>.
- Kong, Y.L., Gupta, M.K., Johnson, B.N., McAlpine, M.C., 2016. 3D printed bionic nanodevices. *Nano Today* 11, 330–350. <https://doi.org/10.1016/j.nantod.2016.04.007>.
- Krieger, K.J., Bertollo, N., Dangol, M., Sheridan, J.T., Lowery, M.M., O'Cearbhaill, E.D., 2019. Simple and customizable method for fabrication of high-aspect ratio microneedle molds using low-cost 3D printing. *Microsyst. Nanoeng.* 5, 42. <https://doi.org/10.1038/s41378-019-0088-8>.
- Leirs, K., Tewari Kumar, P., Decrop, D., Pérez-Ruiz, E., Leblebici, P., Van Kelst, B., Compennolle, G., Meeuw, H., Van Wesenbeeck, L., Lagatie, O., Stuyver, L., Gils, A., Lammertyn, J., Spasic, D., 2016. Bioassay development for ultrasensitive detection of influenza A nucleoprotein using digital ELISA. *Anal. Chem.* 88, 8450–8458. <https://doi.org/10.1021/acs.analchem.6b00502>.
- Li, F., Zheng, Y., Yang, M., Zhang, Y., Pu, Q., 2022. A triple-layer microchannel array chip with micro through-holes for smartphone based point-of-care testing of biomarker. *Sensor. Actuator. B Chem.* 351, 130963. <https://doi.org/10.1016/j.snb.2021.130963>.
- Liu, H., Zhang, H., Han, W., Lin, H., Li, R., Zhu, J., Huang, W., 2021. 3D printed flexible strain sensors: from printing to devices and signals. *Adv. Mater.* 33, 2004782. <https://doi.org/10.1002/adma.202004782>.
- Mi, S., Du, Z., Xu, Y., Sun, W., 2018. The crossing and integration between microfluidic technology and 3D printing for organ-on-chips. *J. Mater. Chem. B* 6, 6191–6206. <https://doi.org/10.1039/C8TB01661E>.
- Mostafa, K.G., Nobes, D.S., Qureshi, A.J., 2020. Investigation of light-induced surface roughness in projection micro-stereolithography additive manufacturing (PµSLA). *Proced. CIRP* 92, 187–193. <https://doi.org/10.1016/j.procir.2020.05.177>.
- Muyldermans, S., 2021. Applications of nanobodies. *Annu. Rev. Anim. Biosci.* 9, 401–421. <https://doi.org/10.1146/annurev-animal-021419-083831>.
- Okamatsu, M., Hiono, T., Kida, H., Sakoda, Y., 2016. Recent developments in the diagnosis of avian influenza. *Vet. J.* 215, 82–86. <https://doi.org/10.1016/j.tvjl.2016.05.007>.
- Schito, M., Peter, T.F., Cavanaugh, S., Piatek, A.S., Young, G.J., Alexander, H., Coggin, W., Domingo, G.J., Ellenberger, D., Ermantraut, E., Jani, I.V., Katamba, A., Palamouni, K.M., Essajee, S., Dowdy, D.W., 2012. Opportunities and challenges for cost-efficient implementation of new point-of-care diagnostics for HIV and tuberculosis. *J. Infect. Dis.* 205, S169–S180. <https://doi.org/10.1093/infdis/jis044>.
- Shen, Z., Xiang, Y., Vergara, S., Chen, A., Xiao, Z., Santiago, U., Jin, C., Sang, Z., Luo, J., Chen, K., Schneidman-Duhovny, D., Camacho, C., Calero, G., Hu, B., Shi, Y., 2021. A resource of high-quality and versatile nanobodies for drug delivery. *iScience* 24, 103014. <https://doi.org/10.1016/j.isci.2021.103014>.
- Shi, J., Deng, G., Kong, H., Gu, C., Ma, S., Yin, X., Zeng, X., Cui, P., Chen, Y., Yang, H., Wan, X., Wang, X., Liu, L., Chen, P., Jiang, Y., Liu, J., Guan, Y., Suzuki, Y., Li, M., Qu, Z., Guan, L., Zang, J., Gu, W., Han, S., Song, Y., Hu, Y., Wang, Z., Gu, L., Yang, W., Liang, L., Bao, H., Tian, G., Li, Y., Qiao, C., Jiang, L., Li, C., Bu, Z., Chen, H., 2017. H7N9 virulent mutants detected in chickens in China pose an increased threat to humans. *Cell Res.* 27, 1409–1421. <https://doi.org/10.1038/cr.2017.129>.
- Spackman, E., Killian, M.L., 2020. Avian influenza virus isolation, propagation, and titration in embryonated chicken eggs. In: *Spackman, E. (Ed.), Animal Influenza Virus: Methods and Protocols*. Springer US, New York, NY, pp. 149–164.
- Subirada, F., Paoli, R., Sierra-Agudelo, J., Lagunas, A., Rodriguez-Trujillo, R., Samitier, J., 2022. Development of a custom-made 3D printing protocol with

- commercial resins for manufacturing microfluidic devices. *Polymers* 14. <https://doi.org/10.3390/polym14142955>.
- Wang, B., Li, Y., Zhou, M., Han, Y., Zhang, M., Gao, Z., Liu, Z., Chen, P., Du, W., Zhang, X., Feng, X., Liu, B.-F., 2023. Smartphone-based platforms implementing microfluidic detection with image-based artificial intelligence. *Nat. Commun.* 14, 1341. <https://doi.org/10.1038/s41467-023-36017-x>.
- Yang, J., Cheng, Y., Gong, X., Yi, S., Li, C.-W., Jiang, L., Yi, C., 2022. An integrative review on the applications of 3D printing in the field of in vitro diagnostics. *Chin. Chem. Lett.* 33, 2231–2242. <https://doi.org/10.1016/j.ccllet.2021.08.105>.